



Development of a theoretically based thermal model for lithium ion battery pack

Cong Zhu, Xinghu Li, Lingjun Song*, Liming Xiang

School of Transportation Science and Engineering, Beihang University, Beijing 100191, China

HIGHLIGHTS

- We developed a theoretically based thermal model for lithium ion battery pack.
- Increasing current rate has more obvious effect on irreversible heat generation rate.
- The change of SOC mainly affects the reversible heat generation rate.
- There always exists an optimal resistance coefficient for battery pack.
- Reversible heat affects battery temperature only during continuous charge and discharge.

ARTICLE INFO

Article history:

Received 21 June 2012

Received in revised form

7 September 2012

Accepted 8 September 2012

Available online 20 September 2012

Keywords:

Lithium ion battery pack

Thermal model

Heat generation rate

Heat dissipation rate

Reversible heat

ABSTRACT

Based on the porous electrode and concentrated solution theory, a thermal model is developed for lithium ion battery pack. The accuracy of predicted battery temperatures is validated by charge–discharge cycling experiments under natural and forced convection conditions. The heat generation and dissipation rates of battery under different conditions are simulated by the proposed model and the results indicate that: (1) the SOC change has a significant effect on the reversible heat generation rate but has almost no influence on the irreversible heat generation rate; (2) the generation rates of reversible and irreversible heat during charge are almost equal to that during discharge with the same SOC and current rate, but the effect of reversible heat on battery temperature is opposite; (3) for enhancing heat dissipation with a given input power of cooling fan, there always exists an optimum value for the resistance coefficient of battery pack, and the optimal coefficient is increased when the input power of fan increases. In addition, the comparisons between the predicted and measured battery temperature indicate that, the reversible heat has significant influence on battery temperature during continuous charge and discharge, especially under low current rate, but the influence can't be observed during charge–discharge cycles.

© 2012 Elsevier B.V. All rights reserved.

1. Introduction

Lithium ion battery is considered as one of the most ideal energy storage equipment for electric vehicles by virtue of its advantages, such as high power density, long cycle life and low self-discharge rate etc. However, the temperature of lithium ion battery is gradually increased during the charging or discharging process. If battery temperature exceeds the maximum allowed value, the degradation rate of battery life would be accelerated and thermal runaway would even be triggered under some extreme conditions [1]. Therefore, a thermal management system which can maintain battery temperature below the limiting value is required to be specially designed for the lithium ion battery pack

used in electric vehicles. In order to ensure that the battery temperature can be effectively controlled below the limiting value under any driving conditions, it is necessary to fully understand the characteristics of heat generation and heat dissipation of lithium ion battery pack. Numerical modeling is a better way to study the thermal behavior of battery pack than experimental tests with respect to the cost and time consumption. Therefore, developing a thermal model to predict the heat generation rate (HGR) and heat dissipation rate of the single batteries within lithium ion battery pack is helpful and crucial for properly designing the thermal management system.

Several thermal models of lithium ion battery pack have been presented in published literature. According to the difference in calculating the HGR of lithium ion battery, the thermal models can be classified into empirically based, semi-empirically based and theoretically based thermal model. In the empirically based thermal model, the battery HGR is determined purely by the

* Corresponding author. Tel.: +86 10 82339869; fax: +86 10 82316330.

E-mail address: songlingjun@buaa.edu.cn (L. Song).

experimental data of the battery modeled, e.g. the model developed by Park et al. [2] and Mi et al. [3]. Park's model calculated the battery HGR by Joule's law with the internal resistances determined from fitting experimental data of battery at different temperatures, and Mi's model deduced the HGR by experimentally measuring the temperature evolution of battery. The battery HGR in semi-empirically based thermal model is calculated by Bernardi equation [4], e.g. the model established by Chen et al. [5] and Zhang et al. [6]. As the Bernardi equation was derived from the processes of the electrochemical reaction and charge transfer occurring inside lithium ion battery [4], the semi-empirically based thermal model is different from the empirically based thermal model, though the parameters involved in Bernardi equation are also determined from experimental data. In the theoretically based thermal model the battery HGR is obtained from electrode reaction mechanism, e.g. the model proposed by Smith et al. [7] calculated the HGR of lithium ion battery based on the porous electrode and concentrated solution theory.

Since the reliability of battery HGR is completely dependent on experimental data, the application of empirically based thermal model is limited to specific battery packs. The semi-empirically based thermal model has wider application scope, but the model accuracy needs to be improved because of the assumption of neglecting the spatial variations of parameters such as reaction current density, active material concentrations etc. in electrodes, which could lead to significant errors in estimating battery HGR [8]. The theoretically based thermal model determines battery HGR on the basis of the universal electrode reaction mechanism and the consideration of the spatial variation of parameters in electrode. Therefore, it has the widest application scope and the highest accuracy among the three types of thermal models. However, most existing research is focused on the theoretical model of single lithium ion battery, and little work has been done on the development of theoretically based thermal model for lithium ion battery pack.

This paper aims to develop a theoretically based thermal model, which can accurately predict the heat generation, heat dissipation and temperature rise of the single cells within lithium ion battery pack. In addition, as the reversible heat neglected in Smith's model [7] is indicated to account for a significant proportion of the total heat generated inside lithium ion battery [9–11], the battery temperatures with and without considering reversible heat as heat source are estimated by the model and compared to the measured temperatures, in an effort to investigate the effect of reversible heat on the model accuracy under different operating conditions.

2. Model development

2.1. Lithium ion battery pack

Fig. 1 shows the components and arrangement of a typical lithium ion battery pack for electric vehicle application. The battery pack mainly consists of N cells connected in series, $(N + 1)$ cooling channels arranged between the cells, deflector plates and cooling fan etc. Under forced convection condition, a negative pressure environment is created inside battery pack by the cooling fan. As a result, cooling air would be drawn into the battery pack through the inlet and guided into the cooling channels by the lower air deflector. With the guidance of the upper air deflector, the heated air would be expelled from battery pack through the outlet. An ideal design of the deflectors can evenly distribute the airflow to provide uniform pressure difference between the inlet and outlet of each channel.

The thermal model is developed to assist in designing the thermal management system of lithium ion battery pack. For a prismatic lithium ion battery shown in Fig. 1, a small temperature gradient in battery can drive a significant amount of heat to be transferred out, because of the big transfer area and small transfer distance in the thickness direction of battery. Therefore, under normal operating condition, the temperature gradient inside battery is generally small enough to neglect its impact on thermal management. To increase the calculation speed of model, the following assumptions are made:

- (1) The heat generation and temperature inside a single cell are assumed to be uniformly distributed, and the thermal capacity and mass of the cells are also assumed to have no difference.
- (2) The pressure difference between the inlet and outlet of every channel is supposed to be the same, and the velocity gradient of the main airflow along cooling channel can be set at zero.
- (3) The inlet air temperature of every channel is equal to the ambient temperature.

According to the law of energy conservation, the temperature change of cell n within the battery pack shown in Fig. 1 can be calculated by the following equation:

$$c_{\text{bat}} m_{\text{bat}} \frac{dT_{\text{bat}}(n)}{dt} = Q_{\text{gen}}(n) - Q_{\text{dis}}(n) - Q_{\text{con}}(n) \quad (1)$$

where $Q_{\text{gen}}(n)$ is the heat generation rate of cell n , $Q_{\text{dis}}(n)$ is the heat dissipation rate of cell n , $Q_{\text{con}}(n)$ is the heat transfer rate between cell

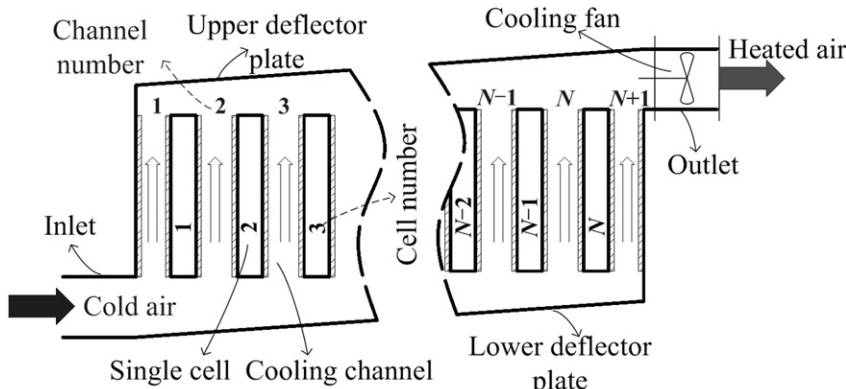


Fig. 1. Schematic view of lithium ion battery pack.

n and adjacent cells, $Q_{\text{con}}(n) = [2T_{\text{bat}}(n) - T_{\text{bat}}(n+1) - T_{\text{bat}}(n-1)]/R_{\text{con}}$, R_{con} is the thermal resistance of the material located between two cells. For a given lithium ion battery pack, the temperature change of cell n mainly depends on $Q_{\text{gen}}(n)$ and $Q_{\text{dis}}(n)$ as expressed by Eq. (1). In the following sections, we will detail the mathematical expressions for them.

2.2. Heat generation within a single battery

The main components of a lithium ion battery are shown in Fig. 2, which include negative current collector, positive current collector, negative electrode, positive electrode and an electron blocking separator. Generally, the negative current collector and positive current collector are made of cuprum and aluminum respectively, and the electrodes and separator are made of porous material and filled with electrolyte composed of organic solvent (ethylene carbonate/dimethyl carbonate) and lithium salt (LiPF_6). As can be seen from Fig. 2, Li_xC_6 and LiMn_2O_4 are separately used as active material for the negative electrode and positive electrode, and δ_n , δ_p , δ_{sep} are used to represent the thickness of negative electrode, positive electrode and separator respectively. According to the porous electrode theory, electrodes can be divided into solid phase and electrolyte phase. During discharge, lithium ions are extracted from the surface of solid Li_xC_6 particle and electrons are released at the same time, then the lithium ions travel via diffusion and migration through separator to the positive electrode, and the electrons collected at negative current collector flow into external circuit to form discharge current. At last, the lithium ions are intercalated into the solid LiMn_2O_4 particles with the electrons delivered from the external circuit. The transport processes of lithium ions and electrons during charge are inverse to that occurred during discharge. Lithium ions extracted from the surface of LiMn_2O_4 particles intercalate into Li_xC_6 particles with the electrons flowing into negative electrode.

The spatial variation of parameters such as reaction current density, active material concentration etc. in electrodes is mainly caused by the transport processes of lithium ions and electrons.

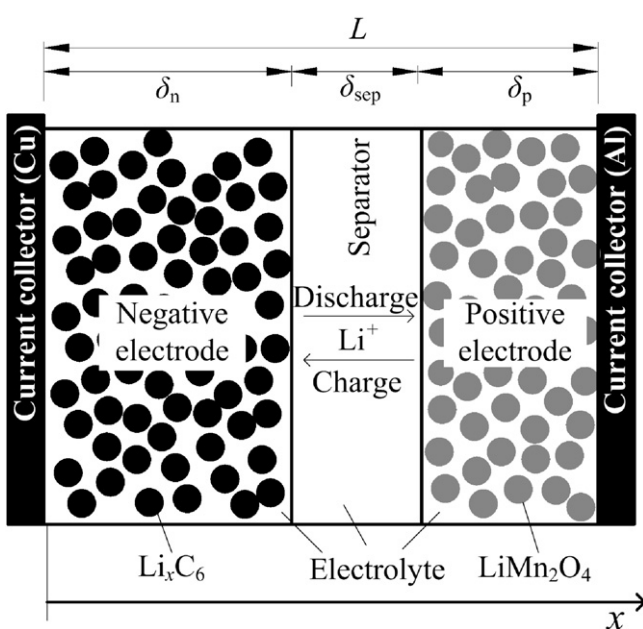


Fig. 2. Schematic of lithium ion battery.

Due to the high electronic conductivity of the current collectors bound to electrodes, the lithium ions and electrons are always transported through the path which is perpendicular to the collectors [12]. Therefore, we only consider the spatial variation of parameters along the thickness direction of electrodes in this paper. Without loss of generality, the following assumptions are also made for the single cell:

- (1) Active material is composed by spherical particles with equal radius and the particles are uniformly distributed in electrodes.
- (2) The diffusion coefficient of lithium ion in solid particles doesn't change with the lithium ion concentration and can be viewed as a constant coefficient.
- (3) The changes of the volume and porosity of the electrodes during charge and discharge can be ignored.
- (4) Side reactions inside battery can also be neglected.

Previous research results indicate that the heat generated inside lithium ion cell can be classified into reversible heat (also named as reaction heat), ohmic heat and polarization heat [11,13–16]. By using the bottom point of the interface between negative electrode and current collector as the origin, and the thickness direction of electrode as the positive direction of x axis, a one dimensional coordinate was established as shown in Fig. 2. Based on the presented assumptions, the computing method for the generation rate of the three types of heat is discussed in the following subsections. It is worth to notice that heat generation rate with positive sign indicates heat release, and that with negative sign indicates heat absorption.

2.2.1. Reaction heat

Due to the difference between the Gibbs free energy of reactant and product, a part of energy is always needed to be released or absorbed in the form of heat to maintain the energy balance of the whole reaction. This part of heat is called reaction heat and its generation rate in the cell shown in Fig. 2 can be calculated by

$$Q_r = -S_e \int_0^L j T_{\text{bat}} \Delta S / (n_e F) dx \quad (2)$$

where j is the bulk density of reaction current in electrode, $j > 0$ means lithium deintercalation while $j < 0$ means lithium intercalation. ΔS is the entropy change of electrode material for a reduction reaction, and can be obtained from the equation $\Delta S = (\partial U / \partial T_{\text{bat}}) nF$, where U is the equilibrium electrode potential, which is a strong function of the SOC and temperature of battery. The relationship between U and SOC can be determined by fitting experimental data at a certain temperature, while the value of $\partial U / \partial T_{\text{bat}}$ is often determined by measuring the variations of U with battery temperature for a given SOC [13]. Fig. 3 provides the values of $\partial U / \partial T_{\text{bat}}$ when lithium intercalation reaction was carried out at different stoichiometries θ in positive electrode (with LiMn_2O_4 active material) and negative electrodes (with Li_xC_6 active material) [11]. As can be seen from Fig. 3, $\partial U / \partial T_{\text{bat}}$ changes significantly with θ . θ is in one-to-one correspondence with the battery SOC, which can be expressed as $\text{SOC} = 100\% \times (\theta - \theta_0) / (\theta_1 - \theta_0)$, where θ_1 is the stoichiometry at 100% SOC and θ_0 is the stoichiometry at 0% SOC. The value of θ is equal to $c_{\text{se}} / c_{\text{smax}}$, where c_{se} is the lithium ion concentration on the surface of the solid particles. Using the particle's center as origin to establish a spherical coordinate, the dynamic change of c_{se} during charge and discharge can be written as

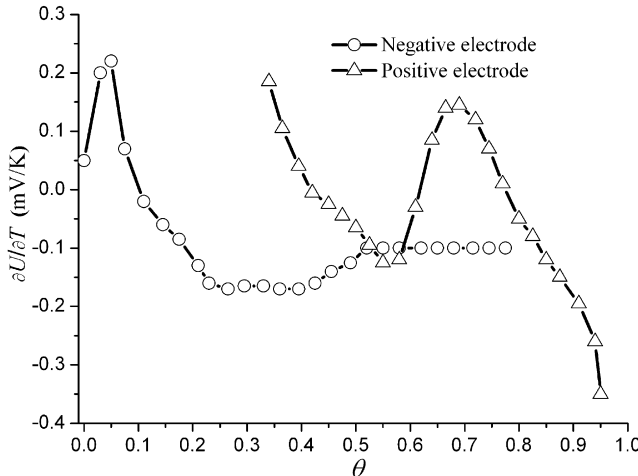


Fig. 3. Variations of $\partial U / \partial T_{\text{bat}}$ with stoichiometry.

$$\frac{\partial c_s}{\partial t} = \frac{D_s}{r^2} \frac{\partial}{\partial r} \left(r^2 \frac{\partial c_s}{\partial r} \right) = D_s \left(\frac{2}{r} \frac{\partial c_s}{\partial r} + \frac{\partial^2 c_s}{\partial r^2} \right) \quad (3)$$

with boundary conditions $(\partial c_s / \partial r)|_{r=0} = 0$, $(\partial c_s / \partial r)|_{r=R_s} = -j / (D_s F_{se})$.

2.2.2. Ohmic heat

Electrons and lithium ions would collide with the transport media in the solid and electrolyte phase during their transport processes. The heat generated by the collisions is called ohmic heat and its generation rate is proportional to the transport fluxes of electron and lithium ion. As described by Ohm's law, the charge transport in solid phase can be expressed by

$$j = \frac{\partial}{\partial x} \left(\sigma^{\text{eff}} \frac{\partial \varphi_s}{\partial x} \right) \quad (4)$$

with boundary conditions $-\sigma^{\text{eff}} (\partial \varphi_s / \partial x)|_{x=0} = \sigma^{\text{eff}} (\partial \varphi_s / \partial x)|_{x=L} = I / S_e$, $(\partial \varphi_s / \partial x)|_{x=\delta_n} = (\partial \varphi_s / \partial x)|_{x=L-\delta_p} = 0$, where I is the working current of battery. $I > 0$ indicates charge while $I < 0$ indicates discharge. Due to the lithium ion diffusion caused by the concentration gradient in electrolyte phase, Ohm's law cannot be directly used to calculate the transport flux of lithium ion. It can be obtained by the following expression derived from concentration theory [17]:

$$\frac{\partial}{\partial x} \left(\kappa^{\text{eff}} \frac{\partial \varphi_e}{\partial x} \right) + \frac{\partial}{\partial x} \left(\kappa_D^{\text{eff}} \frac{\partial \ln c_e}{\partial x} \right) + j = 0 \quad (5)$$

with boundary conditions $(\partial \varphi_e / \partial x)|_{x=0} = (\partial \varphi_e / \partial x)|_{x=L} = 0$, where c_e is the lithium ion concentration in electrolyte phase. The dynamic change of c_e during charge and discharge can be expressed as

$$\frac{\partial (F_e c_e)}{\partial t} = \frac{\partial}{\partial x} \left(D_e^{\text{eff}} \frac{\partial c_e}{\partial x} \right) + \frac{1 - t_+^0}{F} j \quad (6)$$

with boundary conditions $(\partial c_e / \partial x)|_{x=0} = (\partial c_e / \partial x)|_{x=L} = 0$. Besides, the heat generation due to the contact resistance R_c between current collector and electrode can be written as $I^2 R_c$ [7,18]. Therefore, the total generation rate of ohmic heat inside lithium ion battery can be computed by

$$Q_o = S_e \int_0^L \left[\sigma^{\text{eff}} \left(\frac{\partial \varphi_s}{\partial x} \right)^2 + \kappa^{\text{eff}} \left(\frac{\partial \varphi_e}{\partial x} \right)^2 + \kappa_D^{\text{eff}} \frac{\partial \ln c_e}{\partial x} \frac{\partial \varphi_e}{\partial x} \right] dx + I^2 R_c \quad (7)$$

2.2.3. Polarization heat

Under open circuit condition, the activation energy barrier needed to be overcome for deintercalation reaction is equal to the one needed for intercalation reaction. Only when the balance of activation energy barrier is broken, can the net current be produced at the interface between solid phase and electrolyte phase. The energy used to break the barrier balance during charge and discharge would be released in the form of heat at last. The heat is called polarization heat and can be expressed by

$$Q_p = S_e \int_0^L j \eta dx = S_e \int_0^L j (\varphi_s - \varphi_e - U) dx \quad (8)$$

where η is the activation overpotential. The change of activation energy barrier can be described by η . For example, $\eta > 0$ indicates the barrier needed to be overcome for deintercalation reaction would decrease $\alpha_a n_e F \eta$ and the one needed to be overcome for intercalation reaction would increase $\alpha_c n_e F \eta$, while $\eta < 0$ means the former one would increase $-\alpha_a n_e F \eta$ and the later one would decrease $-\alpha_c n_e F \eta$. $\eta = 0$ indicates the barriers are unchanged. α_a and α_c are the anodic and cathodic transfer coefficients respectively. The relationship between η and j can be written as

$$j = S_e i_0 \left[\exp \frac{\alpha_a F}{RT_{\text{bat}}} \left(\eta - \frac{R_{\text{SEU}} j}{S_e} \right) - \exp \frac{-\alpha_c F}{RT_{\text{bat}}} \left(\eta - \frac{R_{\text{SEU}} j}{S_e} \right) \right] \quad (9)$$

where i_0 is the exchange current density and can be determined by

$$i_0 = kF(c_e)^{\alpha_a} (c_{se})^{\alpha_c} (c_{smax} - c_{se})^{\alpha_a} \quad (10)$$

As discussed in subsection 2.2.1, there is a one-to-one correspondence between the c_{se}/c_{smax} and battery SOC. Thus, the exchange current density at the interface of the solid phase and electrolyte phase is closely related to SOC according to Eq. (10).

2.3. Heat dissipation of a single battery

Cooling air is drawn into lithium ion battery pack to cool the single cells through the suction effect created by cooling fan. When the air flows past cooling channel, a thermal boundary layer (TBL) would be formed at the channel wall as shown in Fig. 4. Air temperature in the TBL changes rapidly from the wall temperature (cell temperature) to the temperature of main airflow, and the distance from the wall to the point where the air temperature is 99% of the main airflow temperature is defined as the thickness of TBL. Due to the temperature gradient established in TBL, heat transfer will occur between the channel wall and the air adjacent to it. According to the variations of the thickness of TBL and the heat transfer in TBL, the cooling channel can be divided into thermal entrance region and thermally developed region [19]. In the thermal entrance region, the TBL is growing thicker and the local heat transfer coefficient is decreased along channel, while in the thermally developed region the TBL occupies the entire flow area and the local heat transfer coefficient becomes constant. Considering that the geometric feature of the rectangular cooling channel is similar with that of a flat plate, the temperature profile in TBL in the thermal entrance region can be approximated by a cubic polynomial [19]. With the 2D coordinate shown in Fig. 4, the air temperature in TBL can be described by

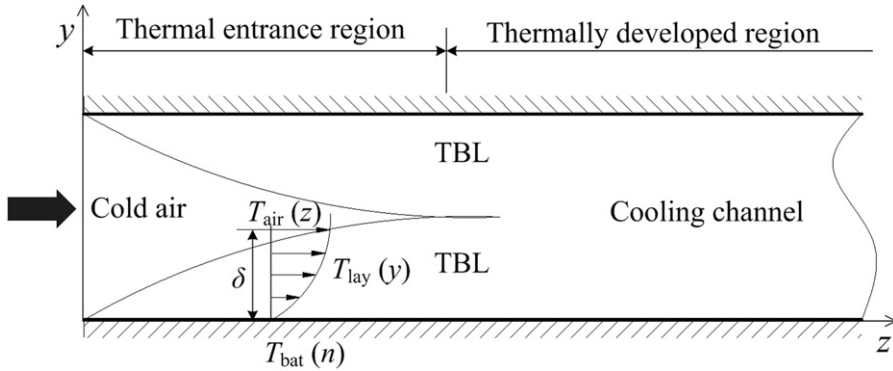


Fig. 4. Development of the thermal boundary layer in cooling channel.

$$T_{\text{lay}}(y) = ay^3 + by^2 + cy + d \quad (11)$$

with boundary conditions $T_{\text{lay}}(0) = T_{\text{bat}}$, $(\partial^2 T_{\text{lay}} / \partial y^2)|_{y=0} = 0$, $T_{\text{lay}}(\delta) = T_{\text{air}} (\partial T_{\text{lay}} / \partial y)|_{y=\delta} = 0$. Substituting Eq. (11) into the four boundary conditions, we get $a = (T_{\text{bat}} - T_{\text{air}})/(2\delta^3)$, $b = 0$, $c = 3(T_{\text{air}} - T_{\text{bat}})/(2\delta)$, $d = T_{\text{bat}}$. With regard to the local heat transfer in channel, the heat carried away by airflow is equivalent to the heat conducted through TBL. Thus, the local heat transfer coefficient h in the thermal entrance region can be expressed as

$$h = -\lambda_{\text{air}} \frac{\partial T_{\text{lay}}}{\partial y} \Big|_{y=0} / (T_{\text{bat}} - T_{\text{air}}) = -\lambda_{\text{air}} c / (T_{\text{bat}} - T_{\text{air}}) = \frac{3\lambda_{\text{air}}}{2\delta} \quad (12)$$

h keeps constant in the thermally developed region, and can be determined by substituting the local thickness of TBL at the interface of the thermal entrance and thermally developed region into Eq. (12). Distributions of the local thickness of TBL $\delta(n, z)$ and local temperature of main airflow $T_{\text{air}}(n, z)$ in the cooling channel n can be expressed as follows:

$$\delta(n, z) = 4.518 \text{Re}_z^{-1/2} \text{Pr}^{-1/3} z \quad (13)$$

$$T_{\text{air}}(n, z) = T_{\text{amb}} + \frac{A_{\text{ch}}}{c_{\text{air}} \rho_{\text{air}} q_{\text{air}}} \int_0^z h(n) [T_{\text{bat}}(n) + T_{\text{bat}}(n-1) - 2T_{\text{air}}(n)] dz \quad (14)$$

where Re_z is the local Reynolds number, $\text{Re}_z = u_{\text{air}} z / v_{\text{air}}$, u_{air} is the velocity of main airflow. Since the airflow in the cooling channel of battery pack is generally laminar, u_{air} is directly proportional to the pressure drop over channel [20]. q_{air} is the volume flow rate of air moving through channel. According to the assumption (2) mentioned in Section 2.1, the pressure drop over channel is proportional to the total pressure drop across battery pack, and q_{air} is equal to $1/(N+1)$ of the total airflow rate.

For the air-cooled thermal management system of lithium ion battery pack, the total volume flow rate, Q_{air} , and pressure drop, ΔP_{sys} , of the air flowing across pack are determined by the operating point of cooling fan. Generally, the fan operating point, which is dependent on the rotational speed of fan n_{fan} and resistance coefficient of battery pack R_{sys} , is obtained by determining the intersection of fan characteristic curve and system resistance curve. Fig. 5 shows the fan operating points at different values of n_{fan} and R_{sys} . As can be seen from the figure, with increasing fan speed, both flow rate and pressure drop at the fan operating point are

increased; with increasing resistance coefficient, the pressure drop at the fan operating point is also increased but the flow rate would be decreased. Therefore, the critical parameters affecting heat dissipation are the rotational speed of cooling fan and the resistance coefficient of battery pack. As the fan speed is proportional to the fan input power P_{fan} , the mathematical relationship between n_{fan} and P_{fan} can be easily determined by fitting experimental data. On the other hand, the resistance coefficient is related to all the structural parameters that can affect the pressure loss in battery pack, such as the width, length and flow area of channel, the inclination angles of upper and lower deflector plate and so on. Considering that the main purpose of this paper is to establish a model for predicting the heat generation and dissipation of lithium ion battery within battery pack, the details of modeling the nonlinear and interactive effects of the structural parameters on resistance coefficient would not be discussed here.

In this paper, the values of Q_{air} and ΔP_{sys} at different fan operating points are experimentally determined and used as the model input. Substituting the measured u_{air} and Q_{air} into Eqs. (13) and (14) to calculate the distributions of δ and T_{air} , then the heat dissipation rate of cell n can be written as

$$Q_{\text{dis}}(n) = A_{\text{ch}} \int_0^{L_{\text{ch}}} \{h(n)[T_{\text{bat}}(n) - T_{\text{air}}(n)] + h(n+1)[T_{\text{bat}}(n) - T_{\text{air}}(n+1)]\} dz \quad (15)$$

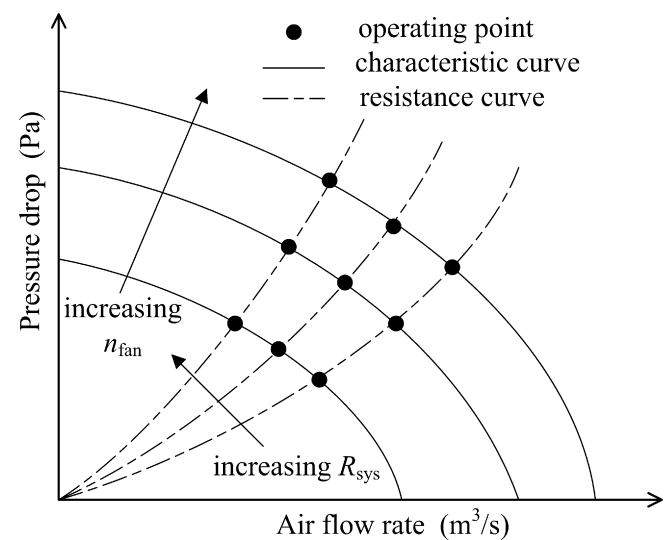


Fig. 5. Operating points of cooling fan at different values of n_{fan} and R_{sys} .

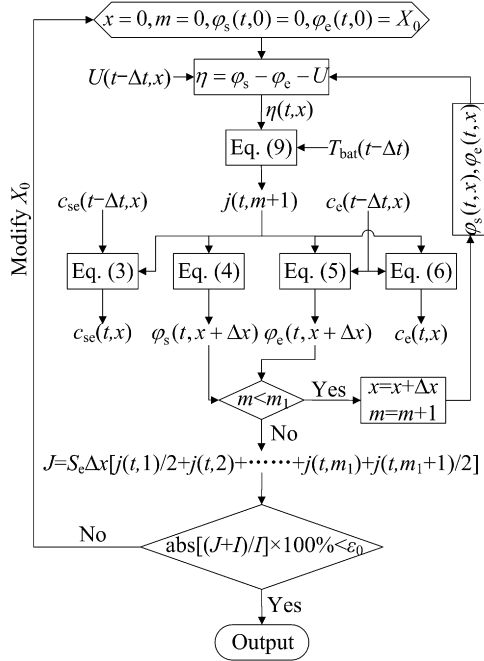


Fig. 6. Flow chart for solving the electrochemical variables.

Table 1
Model parameters for the 144 V/6 Ah lithium ion battery pack.

	Anode	Separator	Cathode
<i>Design parameters</i>			
$\delta_n, \delta_{sep}, \delta_p$ (cm)	50×10^{-4}	25.4×10^{-4}	36.4×10^{-4}
c_e (mol cm $^{-3}$)	1.2×10^{-3}	1.2×10^{-3}	1.2×10^{-3}
$c_{e\max}$ (mol cm $^{-3}$)	16.1×10^{-3}	—	23.9×10^{-3}
R_s (cm)	1×10^{-4}	—	1×10^{-4}
s_e (cm 2 cm $^{-3}$)	1.74×10^4	—	1.5×10^4
R_c (Ω)		1.6×10^{-3}	
S_e (cm 2)		1.0452×10^4	
<i>Kinetic, thermodynamic and transport parameters</i>			
α_a, α_c	0.5	—	0.5
θ_0	$0.11^{[E]}$	—	$0.914^{[E]}$
θ_1	$0.66^{[E]}$	—	$0.42^{[E]}$
D_s^{eff} (cm 2 s $^{-1}$)	4.97×10^{-7}	9.19×10^{-7}	4.93×10^{-7}
D_e (cm 2 s $^{-1}$)	2.0×10^{-12}	—	3.7×10^{-12}
k (cm $^{2.5}$ mol $^{-0.5}$ s $^{-1}$)	1.764×10^{-6} ^[11]	—	3.626×10^{-6} ^[11]
κ^{eff} (Scm $^{-1}$)	1.21×10^{-3}	2.24×10^{-3}	1.2×10^{-3}
σ^{eff} (Scm $^{-1}$)	0.58	—	0.05
κ_D^{eff} (Acm $^{-1}$)		$\kappa_D^{\text{eff}} = 2RT_{\text{bat}}\kappa^{\text{eff}}$ $(t_+^0 - 1/F)$	
t_+^0		0.363	
<i>Physical parameters of battery pack</i>			
c_{bat} (J kg $^{-1}$ K $^{-1}$)	$2460^{[M]}$	m_{bat} (kg)	$0.696^{[M]}$
A_{ch} (cm 2)	$311.75^{[M]}$	L_{ch} (cm)	$14.5^{[M]}$
R_{con} (KW $^{-1}$)	$1.711^{[E]}$	—	—

^[M]Manufacturer.

^[E]Estimated.

^[11]Ref. [11].

3. Solution procedure

To solve the distributions of lithium ion concentration and electrical potential in electrodes, we divide the domain shown in Fig. 2 into M control volumes. Using Δx to denote the length of control volume, then the control volume within which reaction can occur is $S_e \Delta x$. It should be noted that, the values of Δx for the electrodes and separator should be properly determined to ensure that the electrode/separator interface can be matched, and that the spatial variation of reaction current density in each control volume is small enough to be neglected.

Fig. 6 gives a flow chart to illustrate the procedure for solving the species concentration and electrical potential in negative electrode. As shown in the figure, the reasonable values of the variables j , c_e , c_{se} , φ_s and φ_e can be obtained by iteratively modifying the initial value of electrolyte phase potential X_0 , until the relative error of current density reaches the preset threshold value

ε_0 . m_1 in the figure is the number of control volumes within negative electrode and is equal to $\delta_n / \Delta x$. Variables in the positive electrode and separator can be solved in the same way, but the values of j and φ_s are set at zero in the range of $\delta_n < x < L - \delta_p$ as there is no reaction occurred in the separator. With the calculation results of j , c_e , φ_s and φ_e , the total heat generation rate, Q_{gen} , of cell n at time t can be calculated by Eqs. (2), (7) and (8), $Q_{\text{gen}}(t, n) = Q_r + Q_o + Q_p$.

The distributions of TBL thickness, heat transfer coefficient and air temperature in cooling channel can be obtained by following steps: (a) substitute the air velocity u_{air} measured at fan operating point into Eq. (13) to calculate the local TBL thickness δ ; (b) utilize δ to calculate the local heat transfer coefficient h by Eq. (12); (c) substitute h and the airflow rate Q_{air} measured at fan operating point into Eq. (14) to compute the local air temperature T_{air} . Based

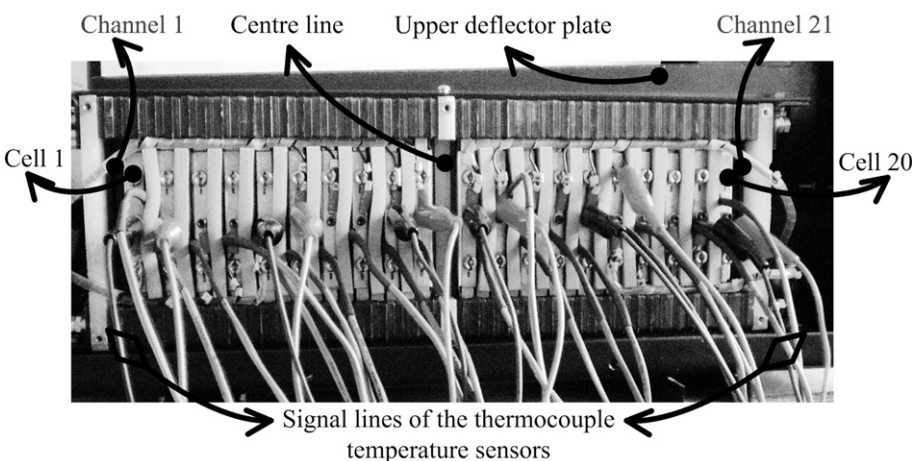


Fig. 7. Lithium ion battery pack and surface mounted thermocouples.

Table 2

Operating conditions of lithium ion battery pack.

	P_{fan} (W)	P_{dis} (kW)	P_{cha} (kW)	T_{amb} (°C)
Case 1	0	5	3	29.5
Case 2	0	10	6	31.3
Case 3	1.33	10	6	30.2
Case 4	2.43	10	6	27.9

on the calculated h and T_{air} , the cell heat dissipation rate $Q_{\text{dis}}(t, n)$ can be determined by Eq. (15). And then, combining $Q_{\text{gen}}(t, n)$ and $Q_{\text{dis}}(t, n)$, the temperature change of cell n can be deduced from Eq. (1).

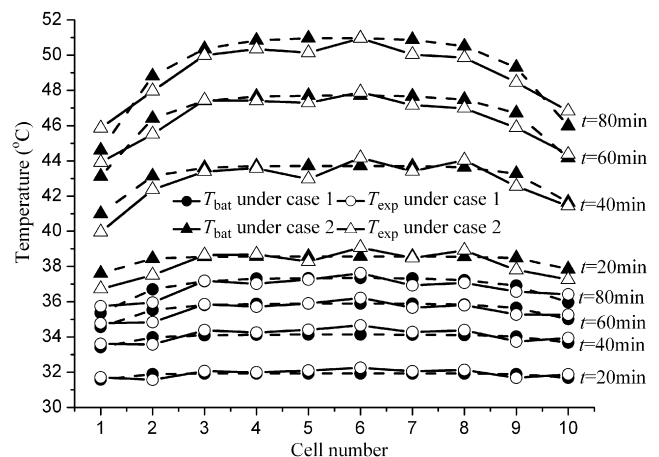
4. Results and discussion

The 144 V/6 Ah lithium ion battery pack given in Fig. 7 is used as the computational domain. As shown in the figure, thermocouple temperature sensors are mounted on the cell surfaces to measure their temperature in real time. The values of model parameters for the battery pack are given in Table 1. In the table, the parameter values without superscript are determined from Ref. [7], and the others are determined from Ref. [11], battery manufacturer or estimated by fitting the model simulation results to experimental data. For the modeling medium, the height and length of the control volume are 12 cm and 2×10^{-4} cm respectively, and the time step size used in the simulation is 0.1 s.

4.1. Model validation

In order to fully validate the effectiveness of the proposed thermal model, the predicted and measured cell temperatures are compared under four different operating conditions given in Table 2. All the operating conditions are composed by a series of charge–discharge cycles. Every cycle incorporates a 10 s constant power discharge, a 40 s rest and a 10 s constant power charge, which is similar to the HPPC test profile specified in the battery test manual [21]. P_{dis} , P_{cha} and P_{fan} in the table represent the discharge power and charge power of battery pack, and the input power of cooling fan respectively. $P_{\text{fan}} = 0$ indicates the battery pack operates under natural convection condition and the local heat transfer coefficient can be fixed at $5 \text{ W m}^{-2} \text{ K}^{-1}$ along the whole cooling channel [22]. At the beginning of the charge–discharge cycling experiments (when $t = 0$), the SOC of battery pack is 50% and all the cell temperatures are equal to the corresponding ambient temperature shown in Table 2.

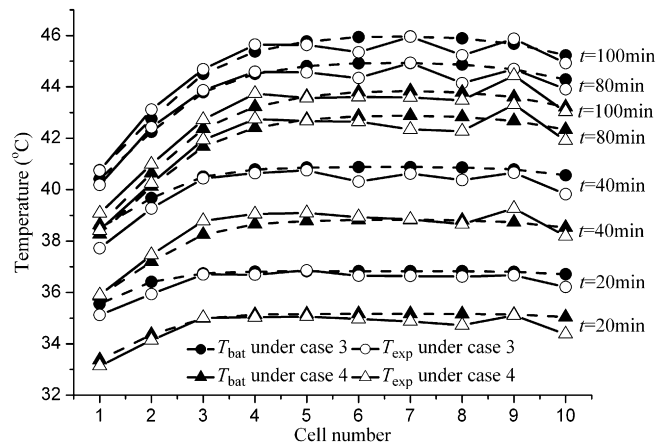
Figs. 8 and 9 show the comparisons between the predicted cell temperature T_{bat} and measured cell temperature T_{exp} under the four operating conditions. Considering that the temperature distribution is almost symmetrical with respect to the center line of battery pack, the figures only give the first 10 cell temperatures. It can be seen that the simulation results agree well with the experimental results, and that the maximum deviation between the predicted and measured temperatures is less than 1 °C, which convincingly proves that the proposed thermal model can accurately simulate the dynamic changes of cell temperature when lithium ion battery pack operates under natural and forced convection conditions. The rising rate of cell temperatures can be efficiently reduced by increasing the input power of cooling fan, but the temperature uniformity across the battery pack is also deteriorated. Therefore, the thermal management system of lithium ion battery pack should be properly designed to balance the temperature rise and uniformity of temperature distribution.

Fig. 8. Comparisons of T_{exp} with T_{bat} under natural convection condition.

4.2. Effects of current rate and SOC on heat generation rate

Fig. 10 shows the variations of heat generation rate when the battery pack with SOC of 50% is charged and discharged at different current rate. Q_{rev} and Q_{irr} in the figure represent the predicted generation rates of reversible and irreversible heat of a single cell respectively, $Q_{\text{rev}} = Q_r$, $Q_{\text{irr}} = Q_o + Q_p$. As expressed by Eq. (2), the generation rate of reaction heat is proportional to the current density, while according to the Joule's law the generation rate of ohmic heat is proportional to the square of current rate. Therefore, as shown in the figure, Q_{rev} increases at an almost constant rate with increasing current rate, but the increasing rate of Q_{irr} is increased gradually.

Fig. 11 presents the variations of Q_{rev} and Q_{irr} when the battery pack with different SOC is charged and discharged at 10 C current rate. It shows that the SOC change affects Q_{rev} obviously but has no significant influence on the Q_{irr} . Since the $\partial U / \partial T_{\text{bat}}$ is strongly dependent on SOC as shown in Fig. 3, the reaction heat generation rate varies significantly with SOC. Due to the exchange current density is closely related to SOC as expressed by Eq. (10), the polarization heat generation rate also changes with SOC for a given current rate. However, the SOC change has no effect on the generation rate of the ohmic heat contributed by the contact resistance between electrode and current collector, which accounts for the biggest ratio of the total irreversible heat. Thus, the change of reaction heat with SOC is well reflected in the variation curve of Q_{rev} , while the change of polarization heat generation rate with SOC is not obvious in the variation curve of Q_{irr} .

Fig. 9. Comparisons of T_{exp} with T_{bat} under forced convection condition.

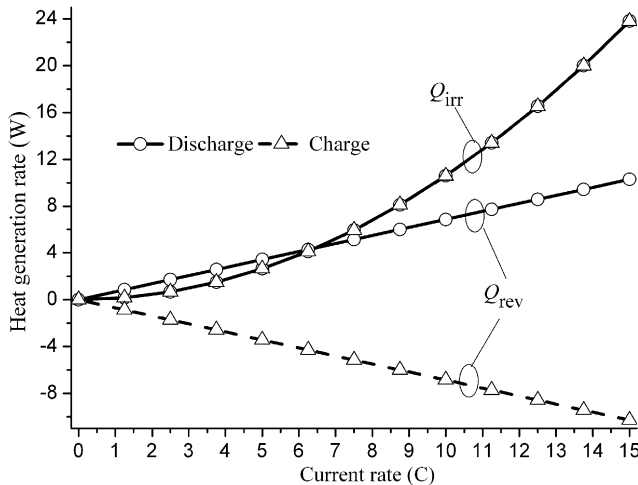


Fig. 10. Variations of Q_{rev} and Q_{irr} with current rate.

Besides, as can be seen from the Fig. 10 and Fig. 11, the variation curve of Q_{irr} during charge is almost completely coincided with the one during discharge, and the variation curves of Q_{rev} are symmetric. When the battery pack with the same SOC is charged and discharged at the same current rate, the number of electrons and lithium ions collided with transport media, and the change extents of the activation energy barriers needed to be overcome for intercalation and deintercalation reaction are almost the same, but the entropy changes of electrodes during charge is exactly opposite to the one during discharge. Hence, the generation rates of reversible and irreversible heat during charge are almost equal to that during discharge, but the signs of the reversible heat generation rates are opposite. Opposite sign means the effect of reversible heat on cell temperature is different, i.e. if the reversible heat generated during charge raised the cell temperature, then that generated during discharge would reduce the cell temperature.

4.3. Effect of resistance coefficient on heat dissipation rate

According to the discussion presented in Section 2.3, the resistance coefficient of battery pack is varied with the structural parameters of cooling channel, and varying resistance coefficient could change the total airflow rate Q_{air} for a given P_{fan} . With the help of the characteristic curve of cooling fan, we can use the

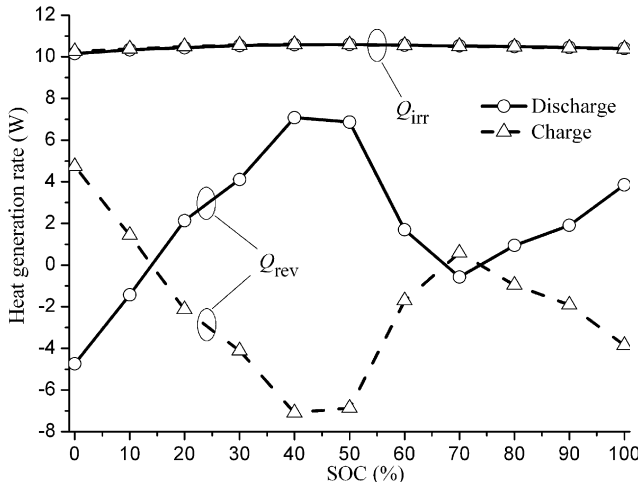


Fig. 11. Variations of Q_{rev} and Q_{irr} with SOC.

change of Q_{air} to describe the variation degree of the resistance coefficient of battery pack. For example, if Q_{air0} denotes the total airflow rate of the 144 V/6 Ah battery pack with its original resistance coefficient, then $Q_{air} < Q_{air0}$ means the resistance coefficient of the battery pack is increased, and the smaller the Q_{air}/Q_{air0} , the higher the resistance coefficient.

Utilizing given Q_{air} and P_{fan} to determine the fan operating point, we can calculate the heat dissipation rate for the battery pack with varied resistance coefficient. Fig. 12 presents the variations of heat dissipation rate of a single cell with resistance coefficient at different values of P_{fan} . The cell temperature and its ambient temperature are equal to 50 and 25 °C respectively. As shown in the figure, there always exists an optimal resistance coefficient for the battery pack such that the heat dissipation rate can reach a maximum value. This can be explained by that, for a given P_{fan} , battery pack with a lower resistance coefficient corresponds to a smaller air velocity in cooling channel, which can result in a lower heat transfer coefficient h as expressed by Eqs. (12) and (13), while battery pack with a higher resistance coefficient corresponds to a smaller airflow rate in the channel, which would lead to a higher air temperature T_{air} as presented in Eq. (14). Therefore, according to Eq. (15), too low or too high resistance coefficient is not beneficial for dissipating heat from battery pack. It can also be seen in the figure, the optimal resistance coefficient is increased when the fan input power increases. This is because the impact of decreasing h on heat dissipation is stronger than that of increasing T_{air} under big input power condition. Thus it can be concluded that when a cooling fan with big input power is installed to provide cooling airflow, the thermal management system of battery pack should be designed to have a high resistance coefficient, in order to make full use of the cooling ability of the fan.

4.4. Effects of reversible heat on model accuracy

The lithium ion battery pack for pure electric vehicle application is often charged or discharged continuously, while the one for hybrid electric vehicle application is always cycled about a relatively fixed SOC. In order to comprehensively evaluate the effects of reversible heat on the model accuracy, the cell temperatures are predicted with and without considering reversible heat as heat source, and compared with the measured cell temperature under different operating conditions.

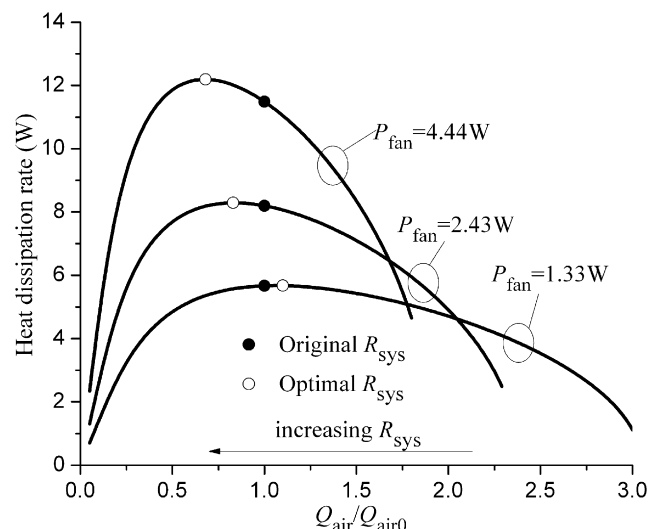


Fig. 12. Variations of Q_{dis} with resistance coefficient.

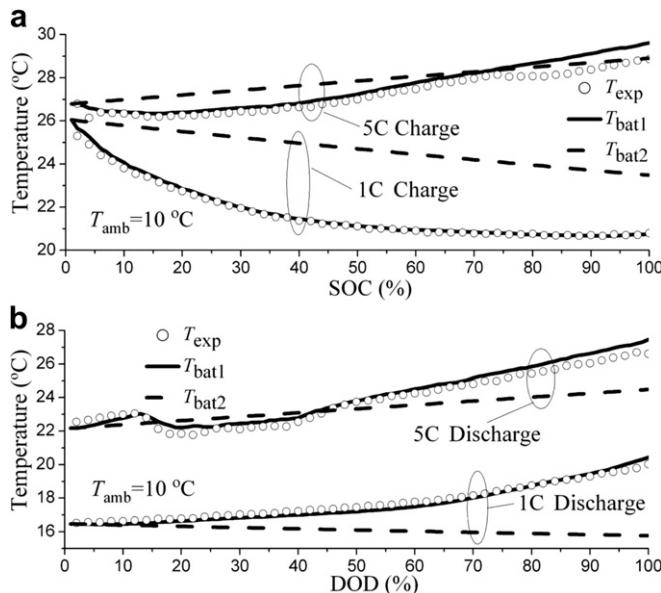


Fig. 13. Comparisons of T_{exp} with T_{bat1} and T_{bat2} during continuous charge and discharge, (a) constant current charge, (b) constant current discharge.

Fig. 13 shows the comparisons of T_{exp} with T_{bat1} and T_{bat2} during constant current charge and discharge of 1 C and 5 C current rate. T_{bat1} is the predicted cell temperature when $Q_{\text{gen}} = Q_{\text{irr}} + Q_{\text{rev}}$ and T_{bat2} is the predicted cell temperature when $Q_{\text{gen}} = Q_{\text{irr}}$. It can be seen that the reversible heat has significant effect on cell temperature when the battery pack is charged or discharged continuously, and the effect is especially obvious under low current condition. This can be explained by the curves shown in Fig. 10. As shown in the figure, the generation rates of reversible and irreversible heat are of the same order under low current condition, so the effect of reversible heat on cell temperature must be greater than that under high current condition, when the irreversible heat has become the dominant heat source.

Fig. 14 depicts the comparisons of T_{exp} with T_{bat1} and T_{bat2} when the battery pack with initial SOC of 50% operates under charge–discharge cycles of 5 C and 10 C current rate. As can be seen from the figure, the reversible heat has little influence on cell temperature under this condition. This is because the reversible heat alternately heat and cool the cell when the battery pack is cycled

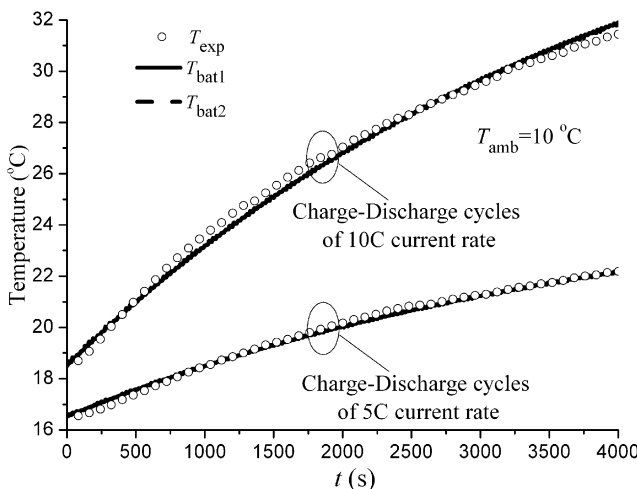


Fig. 14. Comparisons of T_{exp} with T_{bat1} and T_{bat2} during charge–discharge cycles.

about a relatively fixed SOC, the effect of reversible heat on cell temperature is eliminated to some degree.

5. Conclusions

- (1) The proposed theoretically based thermal model is capable of simulating the heat generation and dissipation of lithium ion battery pack. By charge–discharge cycling experiments under natural and forced convection conditions, the accuracy of predicted cell temperatures is validated to within 1 °C.
- (2) The simulation results indicate that, the change of SOC has a significant effect on the reversible heat generation rate but has almost no influence on the irreversible heat generation rate, and the generation rates of reversible and irreversible heat during charge are almost equal to that during discharge with the same SOC and current rate, but the impact of reversible heat on battery temperature is opposite.
- (3) The predictions also show that, for enhancing heat dissipation with a given input power of cooling fan, there always exists an optimum value for the resistance coefficient of battery pack. Although increasing the input power of fan would raise the cost of thermal management, the battery pack is allowed to have a high resistance coefficient, which is helpful in improving the compactness and volumetric power density of battery pack.
- (4) The comparisons between the predicted and measured battery temperatures indicate that, the reversible heat has significant influence on battery temperature during continuous charge and discharge, especially under low current rate, but the influence can't be observed when the battery pack is cycled about a relatively fixed SOC.

References

- [1] J. Robert Selmana, Said Al Hallaja, Isamu Uchidab, Y. Hirano, J. Power Sources 97–98 (2011) 726–732.
- [2] Chanwoo Park, Arun K. Jaura, J. Engines 112 (2003) 1835–1842.
- [3] Chris Mi, Ben Li, Derrick Buck, Naoki Ota, Vehicle Power and Propulsion Conference, IEEE, Texas, 2007, pp. 107–111.
- [4] D. Bernardi, E. Pawlikowski, J. Newman, J. Electrochem. Soc. 132 (1985) 5–12.
- [5] S.C. Chen, C.C. Wan, Y.Y. Wang, J. Power Sources 140 (2005) 111–124.
- [6] Zhuqian Zhang, Li Jia, Nan Zhao, Lixin Yang, J. Therm. Sci. 20 (2011) 570–575.
- [7] Kandler Smith, Chao-Yang Wang, J. Power Sources 160 (2006) 662–673.
- [8] Lin Rao, John Newman, J. Electrochem. Soc. 144 (1997) 2697–2704.
- [9] Xiongwen Zhang, Electrochim. Acta 56 (2011) 1246–1255.
- [10] DongHyup Jeon, Seung Man Baek, Energ. Convers. Manage. 52 (2011) 2973–2981.
- [11] Yonghuang Ye, Yixiang Shi, Ningsheng Cai, Jianjun Lee, Xiangming He, J. Power Sources 199 (2012) 227–238.
- [12] W.B. Gu, C.Y. Wang, J. Electrochem. Soc. 147 (2000) 2910–2922.
- [13] Christophe Forgez, Dinh Vinh Do, Guy Friedrich, Mathieu Morcrette, Charles Delacourt, J. Power Sources 195 (2010) 2961–2968.
- [14] Noboru Sato, J. Power Sources 99 (2001) 70–77.
- [15] Vilayananur V. Viswanathan, Daiwon Choi, Donghai Wang, Wu Xu, Silas Towne, Ralph E. Williford, Ji-Guang Zhang, Jun Liu, Zhenguo Yang, J. Power Sources 195 (2010) 3720–3729.
- [16] Zhiyu Jiang, Jie Zhang, Liangjun Dong, Jihua Zhuang, J. Electroanal. Chem. 469 (1999) 1–10.
- [17] Marc Doyle, John Newman, J. Electrochem. Soc. 143 (1996) 1890–1903.
- [18] Weifeng Fang, Ou Jung Kwon, Chao-Yang Wang, Int. J. Energy Res. 34 (2010) 107–115.
- [19] John H. Lienhard IV, John H. Lienhard V, A Heat Transfer Textbook, third ed., Phlogiston Press, Cambridge Massachusetts, 2006, pp. 286–288, 318–322.
- [20] R.W. Fox, A.T. McDonald, P.J. Pritchard, Introduction to Fluid Mechanics, sixth ed., John Wiley & Sons, New York, 2004, pp. 337–343.
- [21] DOE/ID-11069FreedomCAR Battery Test Manual for Power-Assist Hybrid Electric Vehicles, Idaho National Engineering and Environmental Laboratory, 2003, pp. 89–93.
- [22] A.A. Pesaran, S. Burch, M. Keyser, Proceeding of the 4th Vehicle Thermal Management Systems Conference and Exhibition, London, UK, 1999.

Nomenclature

A_{ch} : heat transfer surface area of cooling channel (m^2)
 c_{bat} : specific heat capacity ($\text{J kg}^{-1} \text{K}^{-1}$)
 c_e : lithium ion concentration in electrolyte phase (mol cm^{-3})
 c_s : lithium ion concentration at the radial position r (mol cm^{-3})

c_{se} : lithium ion concentration at the electrode/electrolyte interface (mol cm^{-3})
 c_{smax} : maximum lithium ion concentration in solid particles (mol cm^{-3})
 D_s : diffusion coefficient of solid phase ($\text{cm}^2 \text{s}^{-1}$)
 F : Faraday's constant, 96487 C mol $^{-1}$
 h : local heat transfer coefficient ($\text{W m}^{-2} \text{K}^{-1}$)
 i_0 : exchange current density (A cm^{-2})
 I : applied current (A)
 j : bulk density of reaction current in electrode (A cm^{-3})
 k : kinetic rate constant ($\text{cm}^{2.5} \text{mol}^{-0.5} \text{s}^{-1}$)
 L_{ch} : channel length (m)
 m_{bat} : battery mass (kg)
 n_e : number of electrons transferred, 1
 P_{fan} : input power of cooling fan (W)
 Pr : Prandtl number of air, 0.7023
 q_{air} : volume flow rate of air moving through channel ($\text{m}^3 \text{s}^{-1}$)
 Q_{air} : total volume flow rate of air across battery pack ($\text{m}^3 \text{s}^{-1}$)
 Q_{con} : heat transfer rate between two adjacent cells (W)
 Q_{dis} : heat dissipation rate (W)
 Q_{gen} : heat generation rate (W)
 Q_o : ohmic heat generation rate (W)
 Q_p : polarization heat generation rate (W)
 Q_r : reaction heat generation rate (W)
 r : radial coordinate along active material particle (cm)
 R : universal gas constant, 8.314 J mol $^{-1}$ K $^{-1}$
 R_c : contact resistance between current collector and electrode (Ω)
 R_{con} : thermal resistance of the material located between two cells (K W $^{-1}$)
 R_s : radius of the solid particles (cm)
 R_{SE} : film resistance at the electrode/electrolyte interface (Ωcm^2)
 R_{sys} : resistance coefficient of battery pack
 s_e : active surface area per electrode unit volume ($\text{cm}^2 \text{cm}^{-3}$)
 S_e : active surface area of electrode (cm^2)
 t : operating time of battery pack (s)
 t^0_s : transference number of lithium ion
 T_{air} : local temperature of main airflow (K)
 T_{amb} : ambient temperature (K)
 T_{bat} : battery temperature (K)
 T_{lay} : air temperature in thermal boundary layer (K)

u_{air} : velocity of main airflow (m s^{-1})
 U : equilibrium electrode potential (V)
 ν_{air} : kinematic viscosity of air ($\text{m}^2 \text{s}^{-1}$)
 ΔP_{sys} : total pressure drop of the air flowing across battery pack (Pa)
 ΔS : entropy change of electrode material ($\text{J mol}^{-1} \text{K}^{-1}$)

Greek letters

α_a, α_c : anodic and cathodic transfer coefficients
 δ : local thickness of thermal boundary layer (m)
 δ_n : thickness of negative electrode (cm)
 δ_p : thickness of positive electrode (cm)
 δ_{sep} : separator thickness (cm)
 ε_e : electrode porosity
 η : activation overpotential (V)
 θ_0 : stoichiometry at 0% SOC
 θ_1 : stoichiometry at 100% SOC
 κ_{eff} : effective ionic conductivity of electrolyte phase (S cm^{-1})
 κ_D^{eff} : effective ionic diffusional conductivity of electrolyte phase (A cm^{-1})
 λ_{air} : thermal conductivity of air ($\text{W m}^{-1} \text{K}^{-1}$)
 σ^{eff} : effective electronic conductivity of solid phase (S cm^{-1})
 φ_e : electrical potential of electrolyte phase (V)
 φ_s : electrical potential of solid phase (V)

Subscripts and superscripts

air : cooling air
 bat : lithium ion battery
 ch : channel
 dis : dissipation
 e : electrolyte phase
 eff : effective
 fan : cooling fan
 gen : generation
 n : negative electrode
 p : positive electrode
 s : solid phase
 sep : separator
 sys : battery pack system